A scalable, Rotating Disc Bioelectrochemical Reactor (RDBER) suitable for the cultivation of both cathodic and anodic biofilms

Max Hackbarth [a], Johannes Gescher [b, c, d], Harald Horn [a, e], Johannes Eberhard Reiner [a,].*

[a] Engler-Bunte-Institut, Water Chemistry and Water Technology, Karlsruhe Institute of Technology (KIT), Engler-Bunte-Ring 9a, 76131 Karlsruhe, Germany

[b] Karlsruhe Institute of Technology (KIT), Institute for Applied Biosciences (IAB), Fritz-Haber-Weg 2, 76131, Karlsruhe, Germany

[c] Karlsruhe Institute of Technology (KIT), Institute for Biological Interfaces (IBG 1), Hermann-von-Helmholtz-Platz 1, 76344 Eggenstein-Leopoldshafen, Germany

[d] Hamburg University of Technology, Institute of Technical Microbiology, Kasernenstraße 12, 21073 Hamburg, Germany

[e] DVGW Research Centre, Water Chemistry and Water Technology, Engler-Bunte-Ring 9a, 76131 Karlsruhe, Germany

** Address correspondence to Johannes Eberhard Reiner, reiner@kit.edu, + 49 721 608 – 4 789 3*

Abstract

This study discusses the construction and operation of a membrane-less bioelectrochemical reactor that employs rotating working electrodes with a surface area of up to 1 m^2. As a proof-of-principle for an aerobic microbial electrosynthesis process, *Kyrpidia spormannii* was cultivated in the reactor. Optical coherence tomography was used to examine the spatial distribution of the cathodic biofilm. After 24 days 87% of the cathode surface was covered with biofilm that was characterized by a radial increase in its biovolume towards the circumcenter of the electrodes reaching up to 92.13 μm^3 μm^{-2}. To demonstrate the versatility of the system, we further operated the reactor as a microbial electrolysis cell employing a co-culture of *Shewanella oneidensis* and *Geobacter sulfurreducens.* Anodic current densities of up to 130 μA cm^{-2} were measured during these batch experiments. This resulted in a maximum production rate of 0.43 liters of pure hydrogen per liter reactor volume and day.

Graphical Abstract

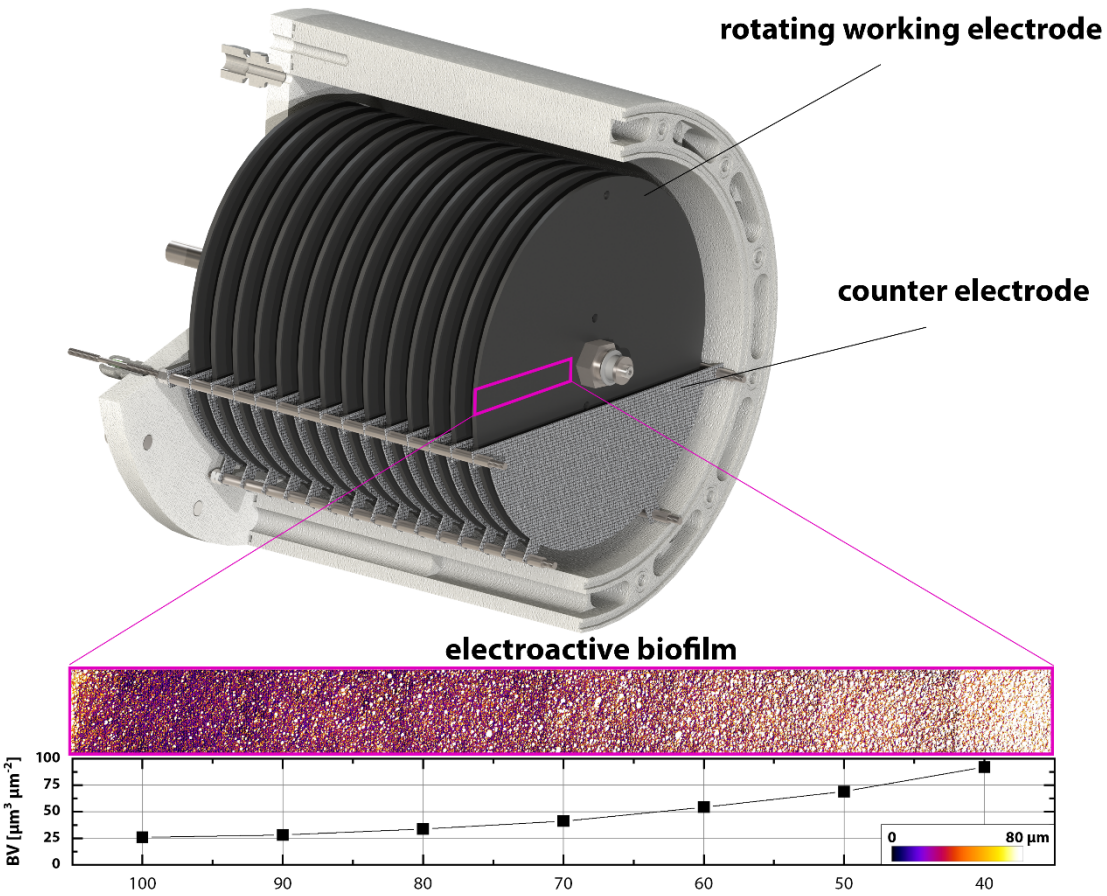

Highlights

- **Construction of a 10 L membrane-less, pressurizable bioelectrochemical reactor**
- **Rotating working electrodes with up to 1 m^2 electrode surface**
- **Electroautotrophic cultivation and quantification of *K. spormannii* biofilms**
- **Initial cell density crucial for successful *K. spormannii* biofilm formation**
- **Anodic operation as MEC with *Shewanella* / *Geobacter* coculture**

Keywords

Pure culture microbial electrosynthesis; microbial electrolysis cell; *Kyrpidia spormannii*; rotating disc bioelectrochemical reactor; rotating biological contactor.

60 **1. Introduction**

61 Tapering off fossil resources by renewable commodities that are based on a circular utilization
62 of resources is key to the transition towards a sustainable economy (Lieder and Rashid, 2016).
63 In this context, future (bio)chemical transformations of raw materials and waste streams must
64 be fueled by renewable electrical energy (Krieg et al., 2018a). The so-called microbial
65 electrosynthesis (MES) is a promising biotechnological example for such a conversion of
66 electricity and carbon dioxide into value-added organic compounds (Nevin et al., 2010). This
67 process relies on electroactive microorganisms that serve as a biocatalyst on the cathode of a
68 bioelectrochemical system (BES) (Logan et al., 2019). By applying a voltage to the BES,
69 typically water is oxidized at the anode into oxygen and protons. Driven by a power source the
70 released electrons are subsequently used either directly or indirectly by the autotrophic,
71 cathodic biofilm as the sole energy and electron source for the reduction of CO_2. Although
72 MES could theoretically outperform abiotic carbon utilization technologies as well as
73 established gas fermentations in some specific applications, the technology is not yet
74 economically feasible on a large scale (Christodoulou and Velasquez-Orta, 2016; Jourdin et
75 al., 2020; Jourdin and Burdyny, 2021; Prévoteau et al., 2020; Wood et al., 2021). However,
76 the novel electroautotrophic species *Kyrpidia spormannii* EA-1^T was isolated from a
77 thermophilic cathodic community recently (Reiner et al., 2018a, 2018b). This thermoacidophilic
78 'Knallgas' bacterium is a natural producer of polyhydroxyalkanoates (PHAs) and was shown
79 to thrive on cathodes as the sole electron and energy source for the reduction of CO_2 (Reiner
80 et al., 2020). Hence, *K. spormannii* is a promising candidate for MES - not only since PHAs
81 are precursors for biodegradable bioplastics - but also due to the organisms comparably good
82 biofilm-formation abilities on cathodes. Thus, it was shown that *K. spormannii* forms robust
83 biofilms with a thickness of well over 100 µm – an important prerequisite for MES as stated
84 recently by Vassilev and colleagues (Barham et al., 1984; Hackbarth et al., 2020; Vassilev et
85 al., 2022). Although it seems to be an intrinsic property of electroautotrophic organisms, the
86 molecular details of extracellular electron uptake (EET) from a cathode are also subject to keen

debate with regard to *K. spormannii* (Jung et al., 2020; Pillot et al., 2022a; Prévoteau et al., 2020; Reiner et al., 2020).

While - with respect to the inanimate components of a MES system - much effort has been put into studying the effect of material and structural properties of electrodes, the development of new and, in particular, scalable reactor concepts for MES has been rather sidelined (Enzmann et al., 2019b; Guo et al., 2015; Kerzenmacher, 2017; Pillot et al., 2022a, 2022b; Zhang et al., 2021). This is in spite of the fact that whether microbial electrochemical technologies (METs) can carve a niche in a future sustainable economy depends strongly on the availability of a suitable reactor technology. Typical reactor systems for the cultivation of electroactive microorganisms in laboratory settings are cube, bottle, or flat-plate-type reactors (Enzmann et al., 2019a; Krieg et al., 2018b). Especially for MES applications, a semipermeable membrane is commonly required to spatially separate anode and cathode compartments. Membranes can be advantageous when extremely high Coulombic efficiencies are desired, as they avoid chemical short circuits caused by diffusion of electrochemically active chemicals (Krieg et al., 2018b). Moreover, due to anodically produced oxygen a membrane is particularly crucial if strict anaerobes, such as acetogenic or methanogenic organisms, serve as cathodic biocatalysts for MES (Gildemyn et al., 2017). However, the utilization of membranes leads to significantly increased surface-specific ohmic losses as a plain result of an increased distance between anode and cathode, but also through diffusion limitations often caused by hardly mixed zones around the membranes. The latter may also result in undesirable pH shifts in the separated compartments (Gildemyn et al., 2017; Guo et al., 2017; Krieg et al., 2018b; Prévoteau et al., 2020; Zeppilli et al., 2016). Finally, most membranes are not autoclavable (according to the manufacturer), sensitive to fouling and prone to leakage due to lack of mechanical stability (Utesch and Zeng, 2018). The above-mentioned disadvantages of membranes, along with the resulting complexity of the reactor set-up, lead to a high-maintenance reactor system which is likely to be very cost-intensive in long-term operation (Kracke et al., 2018).

114 Here, we present the concept of a membrane-less, scalable rotating disc bioelectrochemical
115 reactor (RDBER) for aerobic MES and other pure culture bioelectrochemical applications. The
116 reactor is fully autoclavable and can be pressurized to at least 0.5 bar. Moreover, it is equipped
117 with an optical window allowing for in vivo monitoring of biofilm development on the electrodes
118 using optical coherence tomography (OCT). The systems design is inspired by a so-called
119 rotating biological contactor (RBC) (Hassard et al., 2015). RBC is a fixed-film bioreactor used
120 in wastewater treatment that consists of closely spaced discs that are mounted on a common
121 horizontal shaft and are typically partially submerged in liquid. Cortez and colleagues highlight
122 the low maintenance and operating costs, ease of process control and monitoring, and low
123 land requirements as particular advantages of RBC (Cortez et al., 2008). This is mainly due to
124 the fact that the flow velocity across the biofilm enhancing substrate supply is not achieved by
125 energy-intensive pumping of high volumes or stirring, but by rotation of the biofilm-covered
126 discs. The first steps in the "electrification" of RBCs have already been successfully carried
127 out on a laboratory scale (Cheng et al., 2012, 2011; Rodziewicz et al., 2019; Sayess et al.,
128 2013): Several attempts have been made to use conductive rotating discs as cathode or anode
129 of a bioelectrochemical system. However, these studies consistently focus on the purification
130 of wastewater. Hence, biotechnological requirements for a pure culture MES process (e.g.,
131 working with pure cultures under sterile conditions, control of temperature and pH, or
132 pressurizability to increase the solubility of the gaseous substrates like CO_2) were not
133 considered in the reactor design.

134 The RDBER operates in either anodic (as a microbial electrolysis cell) or cathodic mode with
135 an effective working electrode area of up to 1 m^2 (depending on the number of graphite discs
136 mounted). As a proof of principle for an axenic, aerobic MES-process we cultivated *K.*
137 *spormannii* in the system and correlated the OCT-derived, spacial resolved biovolume of the
138 cathodic biofilm with the radius of the rotating cathodes. Furthermore, we demonstrated that
139 the developed system can also be operated as a microbial electrolysis cell (MEC). In a MEC,
140 electroactive organisms oxidize organic matter into CO_2 and protons, whereby the released
141 electrons are transferred from the organisms to the anode, which serves as a terminal

respiratory electron acceptor. From the anode, the electrons are then transferred to the counter electrode (cathode) by means of a voltage source, in order to reduce protons abiotically into hydrogen. For MEC-operation of the RDBER a co-culture of *Shewanella oneidensis* and *Geobacter sulfurreducens* was cultivated as an anodic biofilm on the rotating working electrodes. Both organisms are well-studied electroactive model organisms for extracellular electron transfer of respiratory electrons to insoluble electron acceptors such as an anode of a MEC (Edel et al., 2022; Korth and Harnisch, 2019; Logan et al., 2019).

Thus, by cultivating defined pure cultures in different operating modes (anodic/cathodic) in each case, we were able not only to demonstrate the general functionality of the system, but also to provide a first insight into the range of possible applications offered by the RDBER as a technological platform for METs.

2. Material and methods

2.1 Reactor Design

The design of the reactor system is illustrated in detail in Fig. 1. The reaction chamber, consisting of the reactor jacket (component b in Figs. 1A and 1C) and two flanges, was designed as a horizontal cylinder made of polypropylene. The inner diameter of the jacket measuring 238 mm and the length of 230 mm result in an inner volume of the reaction chamber of 10 L. An inspection window made of polycarbonate (Fig. 1A, component a) was integrated in the front flange allowing the observation of the foremost working electrode (Figs. 1A and 1C, component d). A circular recess milled in the center of the window serves as a guide and seat for the shaft bearing (component f in Fig. 1A). Figure 1C shows a cross-sectional view of the RDBER illustrating the arrangement of the electrodes in the reaction chamber. The shaft, which was made of high-purity titanium and sealed from the environment by a shaft seal, is located concentrically in the reactor. A precisely aligned shaft bearing in the rear flange, together with the fixed bearing in the front window, ensures that the shaft runs as friction-free and balanced as possible. For compensation of the temperature-related expansion of the shaft relative to the

reaction chamber, the bearing in the rear flange was designed as a floating bearing. The shaft was manufactured as a threaded rod onto which working electrode holders (custom made titanium nuts) are mounted. The working electrode discs made of graphite are clamped between two holders in each case and centered in the process. This ensures that the discs are in contact with the shaft and thus also with the voltage source. In total, up to 14 working electrode discs with a thickness of 3 mm and a diameter of 210 mm can be mounted on the shaft. This corresponds to an active working electrode surface (front and back) of up to 1 m^2 and, relative to the reaction chamber volume, a surface-to-volume ratio of 100 $m^2\ m^{-3}$.

Since in RBC-like systems the cross-flow across the biofilm is adjusted by the rotational speed of the rotating substrate (here the working electrode), a high-resolution stepper motor (component c, Figs. 1A and 1B) was implemented (Lexium MDrive Motion Control, Schneider Electric) on the rear flange. The employment of such a stepper motor allows, in addition to the load-independent control of the rotational speed, the position-accurate visualization of selected locations on the substrate. Apart from the toothed belt wheel required for this purpose, a double leg carbon brush holder (Fig. 1B, component l) with silver-graphite brushes was attached to the end of the titanium shaft (Fig. 1C, component n). Via this brush holder, electrical contact was made from the potentiostat to the rotating shaft and thus also to the working electrodes. The counter electrodes were made of titanium sheet with an iridium mixed oxide coating (platinode type 177, Umicore) in the form of half-rounds (Fig. 1C, component m) and connected to each other by means of four titanium threaded rods (Fig. 1C, component o). Exactly cut pieces of titanium pipe (component p in Fig. 1C) are mounted between each two anode sheets to provide the desired distance between the working and counter electrodes. The distance between anode and cathode amount to 5.5 mm. A total of up to 15 fixed counter electrode sheets with an active area of approx. 0.5 m^2 can be installed in the reaction chamber in this way. The four titanium threaded rods are led out of the reaction chamber through the rear flange (Fig. 1B, component i) and can thus be connected to the potentiostat. Cable bushings made of polytetrafluoroethylene (PTFE) provide the necessary sealing.

In order to supply the growing biofilm with CO_2-enriched media during cathodic operation, the gas-saturated and pre-tempered culture medium was pumped by means of a gear pump with an autoclavable pump head (REGLO-Z Digital, Z-1830 P, Ismatec) (Fig. 1D, component t) from an optional stainless-steel (component r in Fig. 1D) double jacket container via a compression fitting (Fig. 1D, component e) located in the front flange into the reaction chamber. The medium was then circulated in the overall system via two screw fittings (parts h and j in Fig. 1B) located on the rear flange. During operation the volume flow was led via the compression fitting j (Fig. 1B) connected to the reference electrode holder containing an Ag/AgCl reference electrode (part q in Fig. 1D) (SE23I, Meinsberg Sensortechnik). The second screw connection h (Fig. 1B) served as an outlet for any gas that may have formed and collected in the reaction chamber.

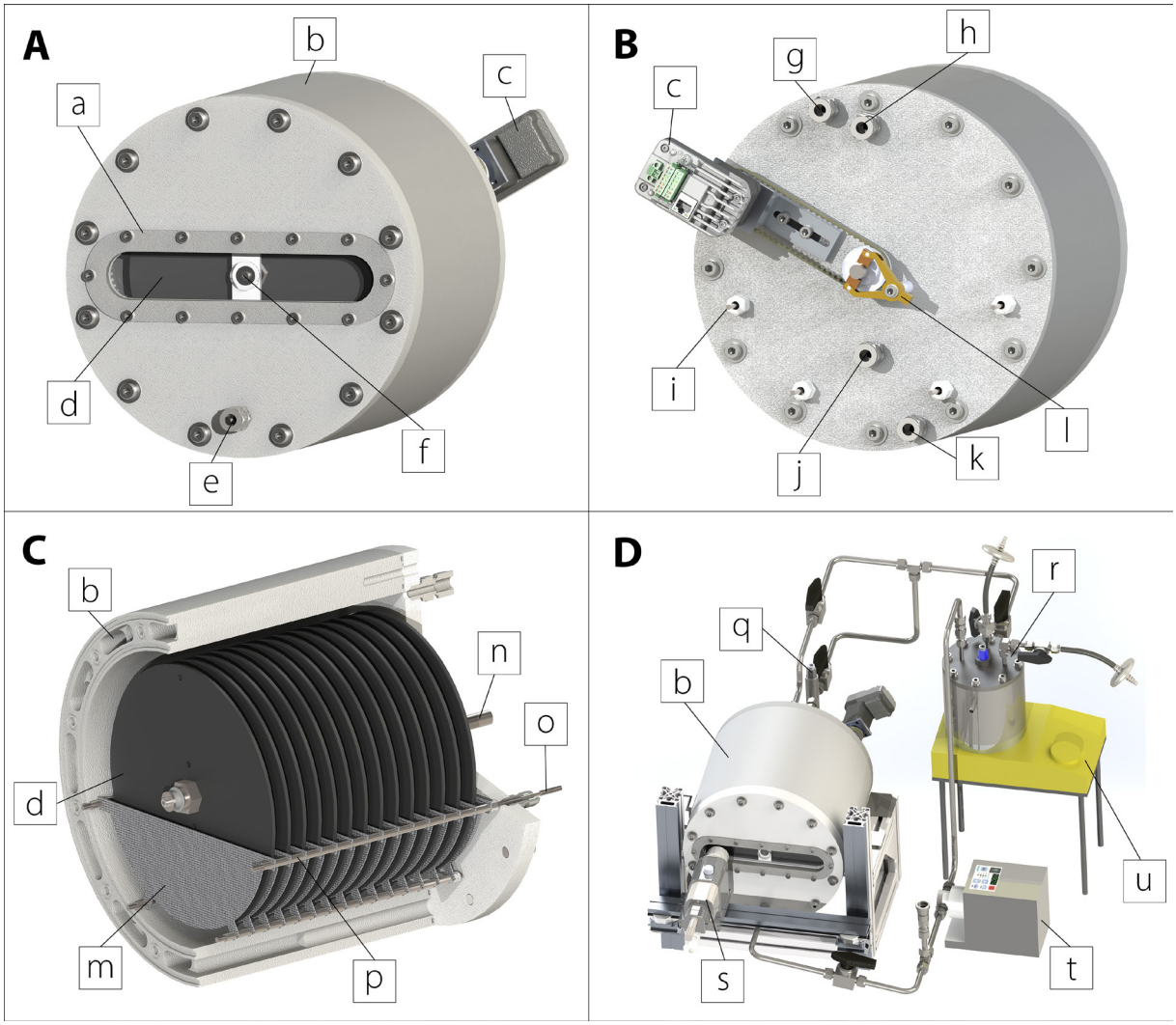

Fig. 1: 3D renderings of the RDBER: (A) Front view of the reaction vessel, (B) rear view of the reaction vessel, (C) cross-section of the reaction vessel, (D) full system with stainless-steel vessel and piping. (a – inspection window, b – reactor jacket, c – stepper motor , d – working electrode disc, e – inlet to reaction chamber, f – shaft journal bearing, g – outlet of heating jacket, h – gas outlet, i – connector to counter electrode, j – outlet of reaction chamber and connection to reference electrode holder, k – inlet to heating jacket, l – carbon brush holder as connector to rotating working electrodes, m – counter electrodes , n – working electrode shaft , o – counter electrode shaft, p – counter electrode spacers, q – reference electrode, r - double jacketed vessel with integrated pH electrode, s – OCT probe head, t – magnetic gear pump, u – magnetic stirrer).

220 To ensure constant temperatures in the reaction chamber, heating channels were milled into
221 the 31 mm thick polypropylene jacket. These channels were flushed with heating liquid and
222 are shown in the cross-section of the reaction chamber (Fig. 1C). Inlet k and outlet g (Fig. 1B)
223 of the heating jacket were placed at the rear flange of the reaction chamber and coupled to a
224 circulation thermostat via clamping ring connections. Simultaneously the growth medium was
225 heated supportively in the optional stainless-steel double jacket vessel during cathodic
226 operation (Fig. 1D, part r). Moreover, the gaseous substrates for electroautotrophic growth
227 were continuously passed through the headspace of the stainless-steel vessel under pressure.
228 The inlet and outlet of the substrate gases are equipped with sterile filters to prevent
229 contamination. By installing a pH electrode (Ceragel CPS71D, Endress + Hauser) in the
230 vessel, the pH value and temperature was logged and the circulation thermostat was regulated.
231 The RDBER was aligned and rigidly fixed on a base frame. Moreover, a holder on which the
232 OCT probe (component s in Fig. 1D) can be fixed was mounted to the base frame.

233

234 **2.2 Strains and preculture conditions**

235 Electroautotrophic experiments were conducted with a population of *K. spormannii* EA-1^T
236 previously adapted to cathodic growth (Jung et al., 2020). The preculture for RDBER
237 experiments was grown from freezer stocks in a modified R2A medium (yeast extract 5 g L^{-1},
238 tryptone 1 g L^{-1}, casamino acids 0.5 g L^{-1}, sodium pyruvate 0.5 g L^{-1}, $MgSO_4 \cdot 7\ H_2O$ 0.05 g L^{-1},
239 K_2HPO_4 0.1 g L^{-1}, MOPS 10 mM - pH 6) at 60 °C without agitation. The heterotrophically grown
240 pre-culture of *K. spormannii* was washed two times with ES-medium (pH 3.5; 10 mM NH_4Cl,
241 2.5 mM NaCl, 0.3 mM KH_2PO_4, 0.12 mM $MgSO_4$, 0.1 mM $CaCl_2$, 1 mL L^{-1} Wolfe's mineral
242 elixir) before inoculating the autoclaved RDBER setup (Reiner et al., 2018a). Depending on
243 the desired planktonic cell number per working electrode surface ratio the initial optical density
244 (OD_{600}) in the RDBER was 0.1 or 0.3 respectively. A counting chamber (Bürker-Türk) was
245 consulted in order to determine the specific cell number per OD_{600} and Volume (an OD_{600} of 1
246 corresponded to 3.16±0.25 * 10^7 *K. spormannii* cells per mL).

247 A mixed culture of the model organisms *Shewanella oneidensis* MR-1 and *Geobacter*
248 *sulfurreducens* PCA was employed as biocatalyst during anodic operation of the RDBER.
249 *S. oneidensis* was precultured aerobically in LB-Medium (Lennox), while the cultivation of the
250 *G. sulfurreducens* preculture was conducted under anoxic conditions in BES-Medium
251 [0.42 g L^{-1} KH_2PO_4, 0.22 g L^{-1} K_2HPO_4, 0.2 g L^{-1} NH_4Cl, 0.38 g L^{-1} KCl, 0.36 g L^{-1} NaCl,
252 0.21 g L^{-1} $MgCl_2$, 11.92 g L^{-1} HEPES – after autoclaving the medium was complemented with
253 1 mL L^{-1} 0.4 mM $CaCl_2$ solution, 10 mL L^{-1} NB trace mineral solution, 1.0 mL selenite–
254 tungstate solution (13 mM NaOH, 17 µM Na_2SeO_3, and 12 µM Na_2WO_4), 10 mL vitamin
255 solution (German Type Culture Collection, DSMZ, media 141) and then sparged in rubber
256 sealed bottles with N_2/CO_2 (80:20 vol%) for 30 minutes]. For preculturing, the BES-medium
257 was complemented with 20 mM sodium acetate as electron donor and disodium fumarate
258 (40 mM) as electron acceptor. The final pH was set to 7.4. Before inoculating the reactor with
259 a mixture of *G. sulfurreducens* and *S. oneidensis* in a 9 to 1 ratio to an initial OD_{600} of 0.1, the
260 cells were washed two times in BES-Medium.

261

262 **2.3 Cultivation of cathodic *K. spormannii* biofilms**

263 After pumping the previously inoculated ES-Medium omitting any organic carbon source
264 (Reiner et al., 2020) into the sterile RDBER, the medium temperature was adjusted to 60 °C.
265 The headspace of the mixing vessel was pressurized to 0.5 bar and continuously flushed with
266 a mixture of 99.5% CO_2 (v/v) and 0.5% O_2 (v/v) while the liquid phase was continuously stirred
267 at 300 rpm. The additional stirring of the medium in the mixing vessel by means of a magnetic
268 stirrer (see component u in Fig. 1D) ensured improved mass transfer of the gases and
269 increased the heat transfer of the heated jacket into the medium. The cultivation medium
270 enriched with the gaseous substrates was pumped through the RDBER at a constant
271 volumetric flow rate of 500 mL min^{-1}. In order to achieve different planktonic cell number per
272 working electrode surface ratios, either only one or all electrodes were mounted (714 cm^2 vs.
273 1 m^2 working electrode surface). The rotational speed of the working electrodes amounted to
274 one revolution per minute. A constant current density of 1 µA cm^{-2} was applied for 24 h

275 immediately after inoculation by means of a potentiostat (Interface 5000P, Gamry Instruments,
276 Warmister, USA). After this initial polarization phase, the current density was set to 3 μA cm^{-2}
277 by the end of the experiment. The experiments were stopped upon detection of no further
278 biofilm increase.
279

280 **2.4 Anodic operation as Microbial Electrolysis Cell**

281 10 L of inoculated BES-medium containing 20 mM sodium acetate and 20 mM sodium lactate
282 as carbon source was pumped in the previously autoclaved RDBER. Chronoamperometric
283 batch experiments were performed at 30 °C and a constant working electrode potential of 0 mV
284 vs. SHE (standard hydrogen electrode) was set. For anodic operation the stainless-steel
285 mixing vessel was omitted while the pipeline was shorted with a pH-electrode holder. Evolving
286 reaction gases (e.g. Hydrogen and CO_2) were collected at the upper outlet h (see Fig. 1B) and
287 led through a MilliGascounter (Ritter, Germany) into a gas sampling bag. Analysis of collected
288 gases was conducted by means of a Micro GC (490 Micro GC, Agilent Technologies,
289 Germany) using two different carrier gases (argon and helium) and two stationary phases (CP-
290 Molsieve 5 Å Plot and PoraPLOT U J&W GC columns, Agilent Technologies, Germany).
291 Moreover, liquid samples were taken twice a day in order to quantify the concentration of
292 organic acids by means of a Metrohm 881 Compact Pro Ion Exchange Chromatograph with a
293 Metrosep Organic Acids 250/7.8 column (Metrohm, Switzerland).

294

295 **2.5 OCT imaging and digital image processing**

296 A GANYMEDE II spectral domain OCT system (Thorlabs GmbH, Dachau, Germany) equipped
297 with a LSM04 objective lens was employed for 3D biofilm visualization (Thorlabs GmbH,
298 Dachau, Germany). Prior to each OCT acquisition, the stepper motor was consistently halted
299 in the same pre-assigned position. Together with the fixed position of the OCT probe holder,
300 this allowed reproducible visualization of a selected radial cathode section. OCT 3D data sets
301 (C-scans) were acquired regularly over the visualizable radial area (see Fig. 2). Each spot was

scanned with a size of 10.0 mm × 6.0 mm × 2.0 mm (L × W × H) and pixel resolutions of 8 µm px^{-1} (lateral, xy-plane) and 2.06 µm px^{-1} (axial, z-direction). Adjacent OCT data sets were then stitched to depict the whole radius of the cathode. The generated OCT datasets were then analyzed, merged, and finally assembled into a height profile (6 mm × 70 mm; H × W). The visualized rectangular area was then trimmed into an isosceles trapezoid for final evaluation. The trapezoid represents a circular sector of the round disc, which abuts the outer radius of the substrate and was shortened to 70 mm by cutting off the tip. 110 of these trapezoids could thus be approximately combined to form a circular ring with an outer diameter of 21 mm and an inner diameter of 70 mm. Finally, the mean biovolume $\overline{BV}$, the mean accumulation rate $\overline{BV}^*$, and the mean coverage $\overline{SC}$ over the radius were determined from the cropped trapezoid (detailed view Figure 2). In addition, the trapezoid was divided into 7 further 10 mm long sub-trapezoids to obtain detailed information about the spatial distribution of biovolume (BV) along the radius of the circular blank. ImageJ (Schneider et al., 2012), operated with in-house made macros (Bauer et al., 2019), was used to calculate topographic representations of the bulk-biofilm interface (height maps) and the structural parameters used for biofilm characterization.

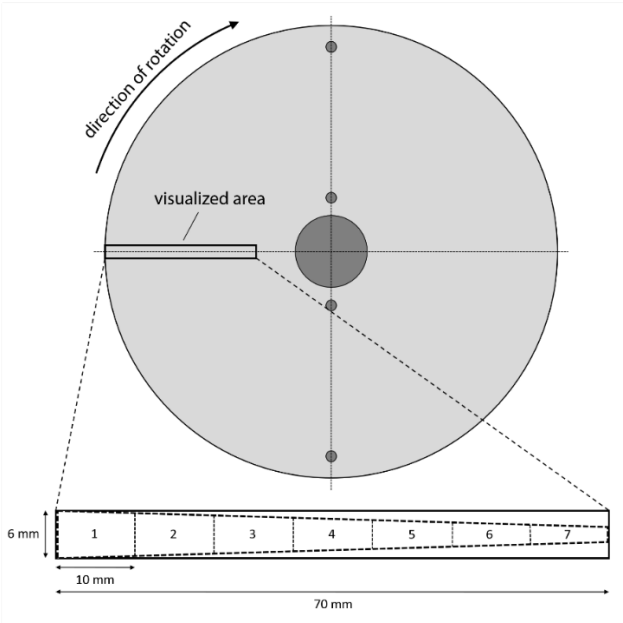

Fig. 2: Representation of the visualized area and the analyzed trapezoidal sections of the generated OCT data sets.

2.6 Parameters for biofilm characterization

The calculation of the biofilm structure parameters - biovolume BV (µm^3 µm^{-2}), mean biovolume $\overline{BV}$ (µm^3 µm^{-2}), mean biofilm accumulation rate $\overline{BV}^*$ (µm^3 µm^{-2} d^{-1}) and mean substratum coverage $\overline{SC}$ (-) was based on height maps according to Wagner and Horn(Wagner and Horn, 2017).

Biovolume BV is defined as the measured biofilm volume V_{BF} (µm^3) per specific area of a single small trapezoid A_{ST} (µm^2)

$$BV = \frac{V_{BF}}{A_{ST}}$$

whereas $\overline{BV}$ is being defined as

$$\overline{BV} = \frac{\sum V_{BFn}}{\sum A_{STn}}$$

Where n indexes the individual small trapezoids.

Mean biofilm accumulation rate $\overline{BV}^*$ corresponds to $\overline{BV}$ derived by time:

$$\overline{BV}^* = \frac{\partial \overline{BV}}{\partial t}$$

Finally, mean substratum coverage $\overline{SC}$ is described as

$$\overline{SC} = \frac{\sum A_{STn} - A_{uc}}{\sum A_{STn}}$$

355 with the area of uncovered substratum A_{uc} (biofilm thickness = 0 µm).

356

357 ## 3. Results and discussion

358 ### 3.1 Cultivation of cathodic *K. spormannii* biofilms

359 In order to prove the functionality of the newly developed reactor concept, two different pure
360 culture cultivations of electroactive microorganisms were performed in the RDBER. Moreover,
361 initial cultivation experiments performed with *K. spormannii* were designed to answer the
362 question of whether an RBC-like reactor could even be a potential technological platform for
363 upscaling a biofilm-based, aerobic MES process that was previously demonstrated in small-
364 scale, custom-made flow cells (Hackbarth et al., 2020; Jung et al., 2020). Thus, as many
365 process parameters as possible were transferred from the established flow cell cultivation to
366 the cultivation of *K. spormannii* in the RDBER for a preliminary cultivation experiment (see
367 Table 1). After several days of reactor operation, OCT analysis of the cathode revealed
368 isolated tower-like structures formed on the cathode. However, their quantity and height
369 decreased sharply again in the course of a few days (Fig. S1). Moreover, the surface coverage
370 of the substratum never exceeded 20% even after one month of cultivation. In summary, no
371 continuous biofilm could be detected on the cathodes by OCT during the preliminary
372 cultivations. When examined more closely, there were two particular process parameters that
373 deviated from the flow cell experiments due to the entirely divergent reactor concept of the
374 RDBER: Firstly, the initial cell number per cathode area, and secondly, the hydraulic retention
375 time in the reaction chamber (0.5 min in the flow-cells compared to 18.4 min in the RDBER).
376 However, since in an RBC-like reactor the flow velocity over the substratum depends on the
377 angular velocity of the substrate rather than the hydraulic residence time (HRT), we assumed
378 that HRT was not likely to be the key process parameter that hindered biofilm growth during
379 the preliminary cultivation experiments. In particular, because care was taken to ensure that
380 the angular velocity of the circular blank at the outermost radius should not exceed the optimum
381 flow velocity for cultivation of *K. spormannii* in the flow cell system. Using the circumference of

382 the circular blanks, it was calculated that a velocity of 11 mm s^{-1} is achieved at the outermost
383 radius at a rotational speed of 1 U min^{-1}, which is within the range of the flow velocity over the
384 cathode in the flow cell system based on the previously conducted CFD simulation (Hackbarth
385 et al., 2020). Hence, we hypothesized, that the 44 times lower initial cell number per cathode
386 surface ratio ($3.4 * 10^9$ cm^{-2} in the flow-cells vs. $7.6 * 10^7$ cm^{-2} for the preliminary RDBER
387 experiments) might be the limiting factor for consistent biofilm growth. Previously it was shown
388 that at the initially uncovered cathode a part of the dissolved oxygen might be abiotically
389 reduced into reactive oxygen species (ROS) (Hackbarth et al., 2020; Jung et al., 2020). As the
390 initial cell number decreases, the cumulative ROS-detoxification capacity of the cells also
391 decreases, possibly preventing a sufficient initial cathode coverage that serves as an insulator
392 to minimize abiotic ROS formation. Therefore, we adjusted the cell number to cathode surface
393 ratio for the subsequent experiments. Besides increasing the initial OD_{600} from 0.1 to 0.3, we
394 also reduced the working electrode area to 700 cm^2, in order to avoid the need of a tremendous
395 amount of preculture, which would not have been cultivatable in our laboratory infrastructure
396 yet. Furthermore, the current density of the system was limited by galvanometry to 1 µA cm^{-2}
397 for 24 h (and then to 3 µA cm^{-2} for the rest of the experiment) to minimize initial ROS-formation.
398 Operation of the RDBER under adapted process conditions now resulted in the formation of
399 nearly continuous *K. spormannii* biofilms covering more than 90% of the cathode. Figure 3
400 shows a timeseries of height maps derived from OCT datasets covering a radial excerpt of the
401 working electrode.

402

403

404

405

406

407 Table 1: Listing of important process parameters comparing the RDBER cultivations of *K. spormannii*
408 performed in this study and flow cell cultivations performed in another study. LSV – Linear sweep
409 voltammetry, CA – Chronoamperometry.

Process parameter	**Flow-cell cultivation (Hackbarth et al., 2020)**	**Preliminary cultivation (this study)**	**Optimized cultivation (this study)**
Medium	ES-medium	Es-medium	Es-medium
pH	3.5	3.5	3.5
Gas mixture	CO_2/O_2 (99.5:0.5)	CO_2/O_2 (99.5:0.5)	CO_2/O_2 (99.5:0.5)
Pressure	1.5 bar	0.5 bar	0.5 bar
Temperature	60 °C	60 °C	60 °C
Circulation pump speed	100 mL min^{-1}	500 mL min^{-1}	500 mL min^{-1}
Volume $_{reaction\ chamber}$	50 mL	8500 mL	9850 mL
Hydraulic retention time	0.5 min	17 min	19.7 min
Flow velocity / angular velocity over / of substratum at r = 210 mm	up to 21 mm s^{-1}	up to 11 mm s^{-1}	up to 11 mm s^{-1}
Electroanalytics	potentiostatic LSV (first 24 h), then CA (-500 mV vs. SHE)	potentiostatic LSV (first 24 h), then CA (-500 mV vs. SHE)	galvanostatic 1 µA cm^{-2} (first 24 h), then 3 µA cm^{-2}
Volume $_{system}$ (incl. pipes, etc.)	850 mL	9500 mL	10850 mL
Initial OD_{600}	0.1	0.1	0.3
Working Electrode Surface	20 cm^2	10000 cm^2	700 cm^2
Initial cell number per working electrode ratio	$1.34 * 10^9$ cm^{-2}	$3.0 * 10^7$ cm^{-2}	$1.47 * 10^9$ cm^{-2}

410

411

412

413

414

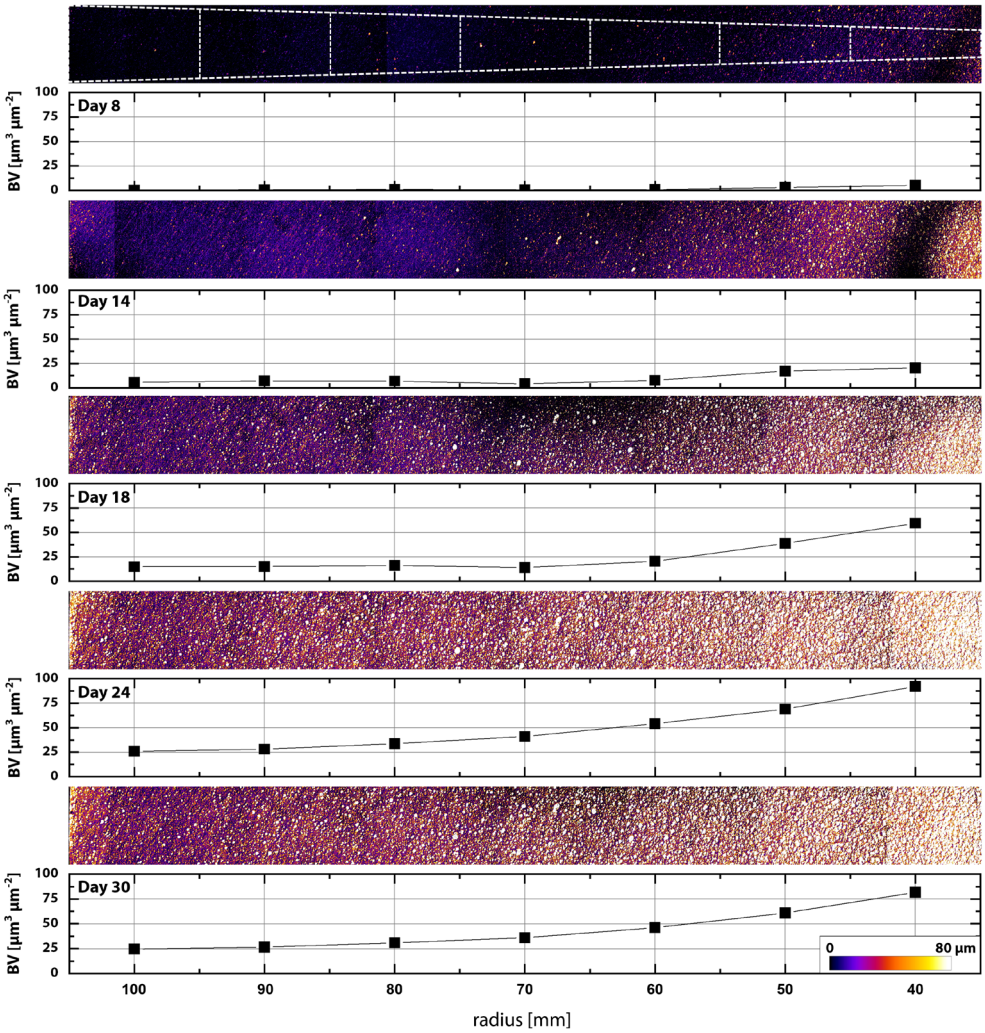

Fig. 3: Time series of selected OCT-derived height maps of the optimized cultivation of *K. spormannii* in the 10 L-RDBER. The same radial section has been visualized on the working electrode in each case in order to show the spatial distribution of the biofilm along the rotating working electrode. Colors are coded from black (0 mm) to white (80 µm). The calculated biovolumes (BV) of the subtrapezoids are shown below the height profiles.

The first visible biofilm structures formed after a lag phase of 8 days near the shaft, i.e. at regions with comparatively low shear stress. A spatially resolved calculation of the local biovolume clearly shows that BV decreases with larger radius towards the edge of the circular blank. So, with an increased angular velocity of the substratum and therefore a higher flow velocity over the biofilm, the biovolume of the *K. spormannii* biofilm is decreasing. After 24 days BV reached the maximum values measured in the course of the experiment in all segments. The maximum BV in the outer region of the cathode averaged 25 $\mu m^3\ \mu m^{-2}$, only about a quarter of the max BV of approximately 92.13 $\mu m^3\ \mu m^{-2}$ observed in the inner visualized region. It should also be mentioned that in an abiotic control experiment, no growth-like precipitation was detected on the cathodes after 24 days. The extent to which the biovolume can be used to draw conclusions about the productivity (i.e., CO_2-fixation rate) of the *K. spormannii* biofilm is not conclusive from this data. Nevertheless, it is known that compressed and denser biofilms generally exhibit higher turnover rates, since more catalytically active biomass is present per biovolume. At the same time, denser biofilm structures might hamper the diffusion of substrates and products within the biofilm (de Beer et al., 1994; Horn and Morgenroth, 2006), whereas the heterogeneity of the biofilm structure will also influence diffusion reaction (van den Berg et al., 2020). Certainly, the increased shear force at increased angular velocity affects the biofilm height to some extent as well. This effect may also be exploited in a future biotechnological process. Thus, a fluctuating and short-term increase of the rotational speed could serve for an optimal harvesting of the biomass from the substratum. In this way, the planktonic biomass could be partially and discontinuously extracted from the reactor, creating a self-sustaining system, since some of the detached cells can recolonize uncovered areas of the substratum. In order to compare the results of the RDBER system with those of the previously published flow cell experiments, calculated $\overline{BV}$ values were fitted by a logistic growth function ($R^2 = 0.98$):

$$\overline{BV} = 40.718 + \frac{(3.055 - 40.718)}{1 + \left(\frac{t}{17.765}\right)^{11.14}}$$

The course of the plotted values of $\overline{BV}$ shows a significantly longer lag phase compared to the flow cell experiments. The highest biofilm accumulation rate of 6 $\mu m^3\ \mu m^{-2}\ d^{-1}$ was reached

452 between days 17 and 18 and was 45% lower compared to the flow cell experiments (see figure
453 6 in (Hackbarth et al., 2020)). Moreover, the maximal achieved mean biovolume in the RDBER
454 system was 42 μm^3 μm^{-2}, which accounted to around 25% of the max. mean biovolume in the
455 flow-cells. The highest coverage of 87% was reached on day 24, with $\overline{SC}$ not describing a
456 steeply increasing degressive course like in the flow-cell experiments, but a linear course until
457 the biofilm finally detached. The biofilm in the RDBER system thus showed a generally weaker
458 and slower growth per area of cathode surface. Notwithstanding, to our knowledge, this data
459 shows the first successful cultivation of an aerobic, electroautotrophic organism in a BES at
460 this scale (700 cm^{-2} working electrode). One of the reasons for the comparatively slow growth
461 of *K. spormannii* in the RDBER was probably the moderate, limited current density (3 µA cm^{-2})
462 - especially in contrast to the measured currents of the flow cell experiments (between 13 and
463 20 µA cm^{-2} at a constant working electrode potential of -500 mV vs. SHE). Although excessive
464 ROS production does not occur if the current density is too low, the biocatalyst may not have
465 enough electrons available for rapid and, above all, complete coverage of the substrate. Thus,
466 in future experiments, the maximum current density should be limited to that extent only during
467 the initial start-up phase and should also be increased as the surface coverage increases.

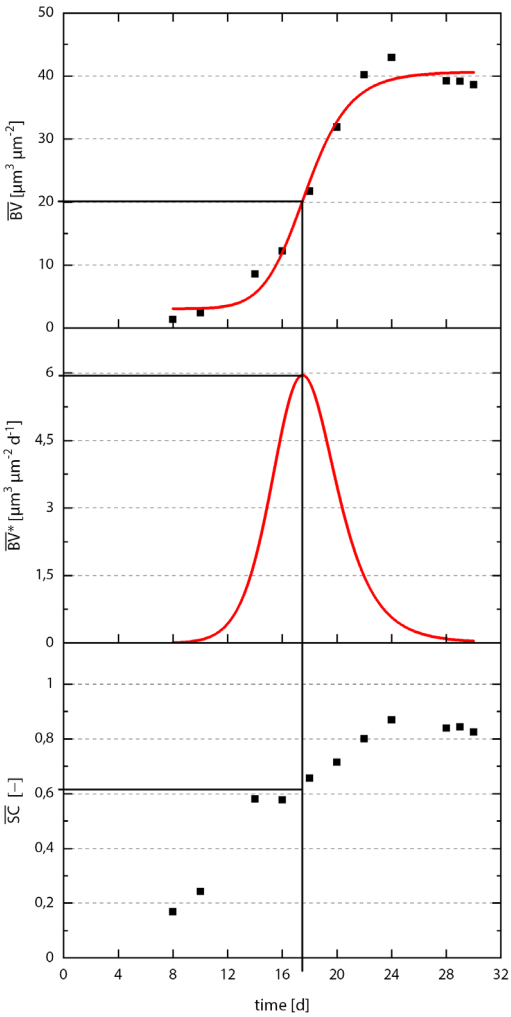

Fig. 4: Plot of calculated biofilm parameters of the optimized cathodic operation of the RDBER over time [mean biovolume ($\overline{BV}$), mean biofilm accumulation rate ($\overline{BV}^*$), and mean substrate coverage ($\overline{SC}$)].

478 In addition to the limitation of the electron donor, reduced substrate availability due to lower
479 solubility of the gaseous substrates at reduced pressure in the RDBER (0.5 bar) compared to
480 the flow cells (1.5 bar) has to be assumed. Indeed, in their computational model of a microbial
481 electrosynthesis process, Cabau-Peinado et al. demonstrated that CO_2 limitations can occur
482 and thus may play a role in low turnover rates of a MES system (Cabau-Peinado et al., 2021).
483 According to the manufacturer, the shaft seal of the titanium shaft in the rear flange is currently
484 the only tender spot that limits the maximum pressure in the system to 0.5 bar. Both the reactor
485 periphery and the entire reactor jacket can be pressurized to at least 1.5 bar. Therefore, future
486 reactor generations should incorporate a shaft seal in the rear bearing that is designed for
487 higher pressure ranges in order to assess the impact of the pressure on the biofilm
488 development in the RDBER. Another approach to reduce a possible substrate limitation may
489 also consist in operating the RDBER in a similar way to an RBC. Here, the reactor would be
490 only half filled with medium, while the gas phase - now present in the reactor chamber - would
491 be flushed with the substrate gases. The fixed film would then move periodically through a
492 highly concentrated CO_2 atmosphere. Furthermore, the actual influence of the HRT in relation
493 to the influence of the rotational speed of the working electrodes on the biofilm growth has to
494 be investigated experimentally in order to exclude a possible growth limitation due to a too low
495 substrate (carbon dioxide) and/or nutrient loading.

496 Based on these experiments, we were able to show that an RBC-like reactor is, in principle, a
497 feasible way to upscale the previously flow cell-based cultivation of *K. spormannii* for bioplastic
498 production from electricity and CO_2. Since the pumping power required for successful
499 cultivation of *K. spormannii* in an upscaled flow cell process would presumably render the
500 overall process quickly uneconomical, an RBC-like reactor might be an interesting option to
501 generate HRT independent crossflow velocities across the working electrode. Furthermore,
502 the cultivation experiments of *K. spormannii* in the RDBER highlighted the crucial role of the
503 start-up phase in aerobic MES processes. The impact of reactive oxygen species should not
504 be underestimated in the development of future MES processes. Therefore, for the necessary
505 development of targeted strategies, it is important to better understand the formation of reactive

506 oxygen species at cathodes under physiological conditions, as well as the different
507 detoxification mechanisms of electroautotrophic microorganisms.

508

509 **3.2 Anodic operation as Microbial Electrolysis Cell**

510 Following the successful cultivation of an electroautotrophic species in the RDBER, we used
511 the reactor to cultivate a defined coculture of *Shewanella oneidensis* and *Geobacter*
512 *sulfurreducens*. The experiments were performed as batch experiments with a full set of the
513 14 working electrodes (here anodes) with a total surface area of 1 m^2. Acetate and lactate
514 served as carbon source with an initial concentration of 20 mM each. The current density at a
515 constant working electrode potential of 0 mV vs. SHE was recorded over the experimental
516 course of roughly 9 days (see Fig 5). After an initial polarization phase of a few hours,
517 characterized by negative current densities most likely due to the depletion of residual oxygen
518 in the system, the current steadily increased until it peaked at 130 µA cm^{-2} after about 4 days.
519 Subsequently, the current density drops again to slowly decrease to about 90 µA cm^{-2} after
520 9 days. Almost uniform in shape runs the graph of the gas evolution rate recorded by means
521 of a MilliGascounter from the gas outlet of the RDBER. The hydrogen fraction in the outflowing
522 gas was examined regularly using a MicroGC and remained almost constant over the entire
523 experimental period (88.1 ± 1.2%). Daily liquid sampling of the reactor's broth was conducted
524 to determine the concentration of the organic acids via ion chromatography.

525

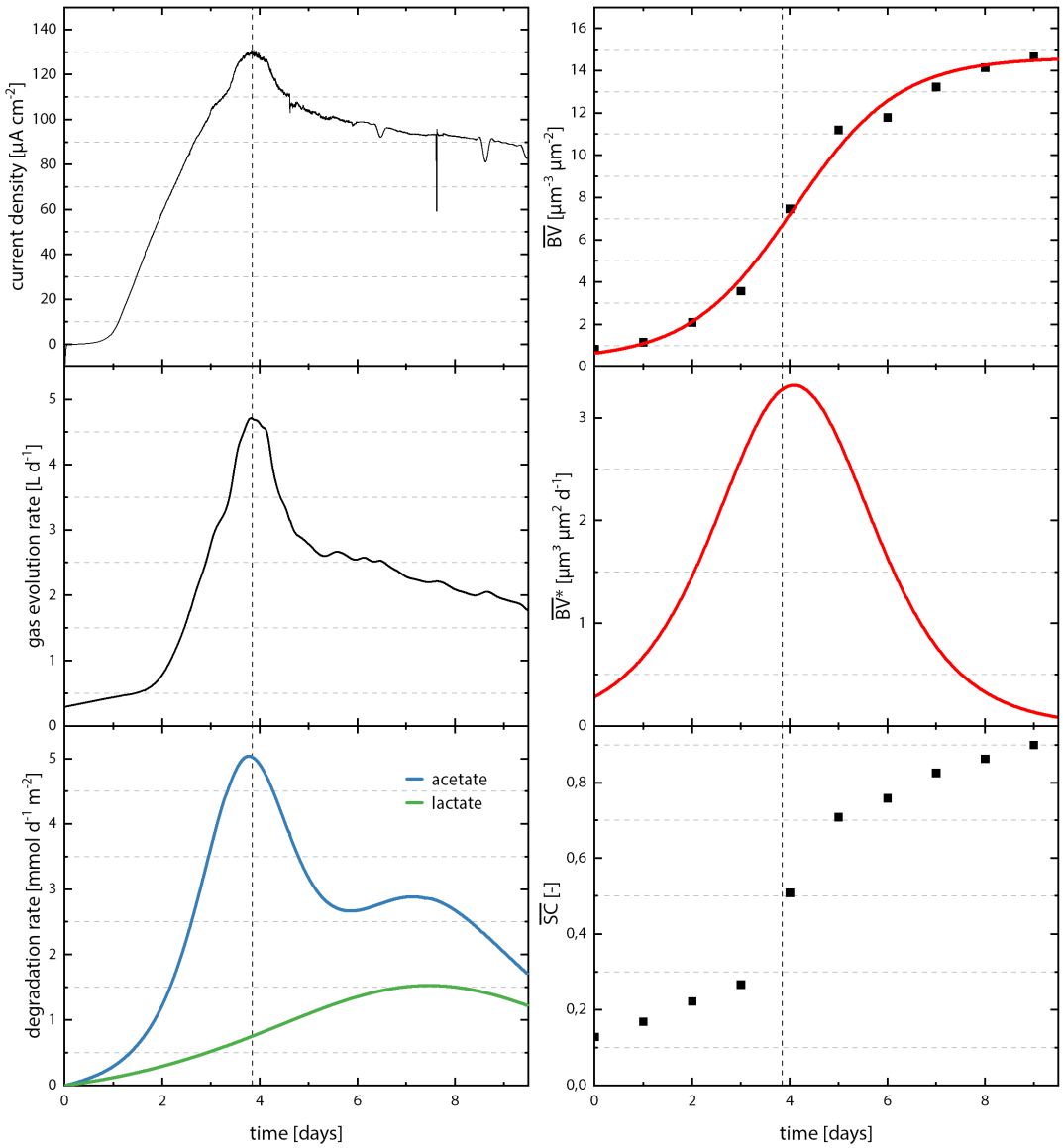

Fig. 5: Correlation of current density, gas evolution rate and substrate specific degradation rate with calculated biofilm parameters obtained during anodic operation of the RDBER. A coculture of *Shewanella oneidensis* and *Geobacter sulfurreducens* was cultivated at a working electrode potential of 0 mV vs. SHE in a MEC-like operation. For a clearer representation, the graphs of current density and gas evolution rate were smoothed with an FFT filter. Raw data of organic acid concentrations, as well as the applied fits (displayed in color), are provided in the Supplementary Material.

The course of the concentration values over time was fitted and derived after time to obtain the specific degradation rates for acetate and lactate, respectively (please refer to Fig. S2 material for original data and fit). In this context, it was important to consider that *Shewanella* degrades one molecule of lactate into one molecule of acetate and CO_2 or formate. Since the acetate concentration did not increase during the experiment, it was therefore assumed that the acetate produced by *Shewanella* was directly metabolized by *Geobacter*. This was taken into account when calculating the specific acetate degradation rate. Since both the peak in current data, and in the gas production rate, correlate with the peak in acetate degradation rate on day 4, these data clearly demonstrate that *Geobacter* is accounting for most of the current production, as *Shewanella* is not capable of metabolizing acetate. The maximum degradation rate for acetate was 5 mmol d^{-1} m^{-2} cathode surface and 1.5 mmol d^{-1} m^{-2} for lactate, respectively. Regular OCT scans of a radial anode section provided the basis for calculating $\overline{BV}$ and $\overline{SC}$. Figure 5 shows the mean biofilm accumulation rate ($\overline{BV}^*$) derived from a logarithmic fit through the calculated $\overline{BV}$ values (R^2 = 0.99):

$$\overline{BV} = 0.343 + \frac{14.646 - 0.343}{1 + 10^{(4.083-t) * 0.404}}$$

The highest biofilm accumulation rate of almost 3 μm^3 μm^{-2} d^{-1} is likewise reached after about 4 days. Again, based on the correlations with the degradation rate, conclusions can be drawn that *Geobacter* cells appear to be the predominant species in the biofilm. This is also consistent with the literature findings that attribute rather modest biofilm capabilities to *Shewanella* compared to *Geobacter* (Engel et al., 2019). After 9 days the anodic biofilm covered around 90% of the observed working electrode surface. Interestingly, the mean surface coverage does not increase linearly as in the cathodic cultivation experiments of *K. spormannii*, but rather logarithmically. Hence, it can be concluded that the growth pattern seen in the cathodic experiments is not so much an intrinsic phenomenon of the RDBER, but probably due to the abiotic formation of ROS on uncovered cathodes described above. On the other hand, or in addition, this distinct growth pattern could also be the consequence of a synergistic effect between the two microorganisms *S. oneidensis* and *G. sulfurreducens* (Engel et al., 2019).

Comparing the performance of the RDBER with other single-chamber upscaling attempts of MECs, it is apparent on the one hand that there is still room for improvement in terms of current densities (up to 130 µA cm^{-2} in this study), but on the other hand the excellent surface to reactor volume ratio (100 m^2 m^{-3}) of the RDBER is worth emphasizing (see Table 2). Although this reached maximum current density is higher than those measured by Huang et al. or by Cotterill et al. (60 µA cm^{-2} and 79 µA cm^{-2} respectively), Wang and colleagues were able to realize tenfold higher current densities using glucose-containing medium, than those achieved in the RDBER (Cotterill et al., 2017; Huang et al., 2019; Wang et al., 2021). Furthermore, this value was surpassed again significantly by the current densities reported by Singh et al. (3400 µA cm^{-2}) (Singh et al., 2021). However, when comparing current densities, it is important to keep in mind that in most MEC studies a constant voltage is applied to the anode and cathode by means of a simple power supply, whereas in our study a potentiometric control of the working electrode potential by means of a potentiostat was used to operate the RDBER. Although a potentiostat allows reproducible electrochemical conditions to be generated, the current densities achieved may be lower than with power supply operation.

Regarding the gas production of the RDBER as another crucial criterion for assessing reactor performance, a maximum hydrogen production rate of 0.43 L L^{-1} d^{-1} (volume hydrogen per reactor volume and day) was achieved on day four. Compared to other single-chamber upscaling attempts, this value is up to several orders of magnitude higher than most of the previously achieved rates (Cotterill et al., 2017; Cusick et al., 2011; Gil-Carrera et al., 2013; Park et al., 2022). Nevertheless, it must be taken into account that some of these studies were conducted using real wastewater as substrate, which generally has lower substrate loading than the synthetic medium used in this study (Cotterill et al., 2017; Cusick et al., 2011; Gil-Carrera et al., 2013). However, under the selected process conditions, the hydrogen production rate achieved with the RDBER does not approach the rates achieved by Wang et al. and Singh et al. (1.67 and 5.9 L L^{-1} d^{-1}, respectively) (Singh et al., 2021; Wang et al., 2021). Finally, when evaluating the discussed performance parameters, it should be noted that the experiments conducted here are only short-term batch tests to validate the functionality of the

system. The above studies were conducted in a continuous operating mode for a significantly longer period of time, up to several months, allowing a more productive biofilm to grow on the working electrode over the longer cultivation period. In addition, the ion chromatographic data also indicate that the biofilm may have already reached a degree of substrate limitation (Fig. S2). Furthermore, it can be assumed that the optimal speed of the working electrodes will have to be determined specifically for each future application of the RDBER and thus for each specific microbial community. Although the comparability of the studies listed in Table 2 proves to be difficult to some extent, since other fundamental parameters (e.g., temperature, pH, electrode materials, electrochemical operating conditions, carbon source and loading rate, HRT, and the microbial community) may differ significantly in addition to the reactor system itself, it nevertheless appears that the RDBER - especially if reactor performance is further enhanced - can compete quite well alongside with existing MEC reactor concepts.

615 Table 2: Comparison of RDBER performance with other up-scaled single-chamber MECs in the
616 literature.

Reference	Volume [L]	WE Material	WE Surface [m^2]	WE Surface to Volume Ratio [m^2 m^{-3}]	Operation Mode	Substrate	Max. H_2 production rate [L_{H2} L_R^{-1} d^{-1}]	Max. current density [µA cm^{-2}]
(Rader and Logan, 2010)	2.5	graphite brushes	-	-	continuous	acetate	0.53	-
(Cusick et al., 2011)	1100	graphite brushes	16.5	15	continuous (HRT 24 h)	winery wastewater	0.19	700
(Gil-Carrera et al., 2013)	10	carbon felt	-	-	continuous (HRT 10 h)	municipal wastewater	0.05	-
(Huang et al., 2019)	40	graphite felt	-	18	continuous (HRT 48 h)	24 mM acetate	0.0039	60
(Wang et al., 2021)	10	carbon cloth	0.42	42	continuous (HRT 62 h)	5 g L^{-1} Glucose	1.67	1370
(Cotterill et al., 2017)	175	graphite felt	34	16.4	continuous (HRT 5 h)	domestic wastewater	0.012	79
(Singh et al., 2021)	10	carbon cloths	1	100	continuous (HRT 12/34 h)	50 mM Acetate 2 g L^{-1} Glucose	5.9	3400
This study	10	graphite discs	1	100	batch (10 days)	20 mM acetate 20 mM lactate	0.43	130

617

618 ## 4. Conclusions

619 In conclusion, the study aimed on the design of a novel, scalable electrochemical reactor
620 concept that meets the requirements of biotechnological pure culture cultivations. During the
621 construction of the single-chamber system, emphasis was laid on a long operating lifetime and
622 low-maintenance operation. The successful cultivation of different electroactive model
623 organisms, both in anodic and cathodic operation, prove on the one hand the basic functionality
624 of the system. On the other hand, we were able to demonstrate that an increase in the working
625 electrode area is not only possible by numbering up individual small reactor systems, as is
626 often the case for METs. Although the experiments discussed here suggest that the RDBER
627 might be a viable reactor concept, in particular for specific niche processes like the aerobic,
628 microbial electrosynthesis, there should be no doubt that more data from long-term studies

under optimized and continuous operating conditions are needed to reliably evaluate the performance of the RDBER compared to other reactor concepts. However, we think that if microbial electrochemical technologies are to become truly competitive, a greater range of creative reactor designs that can be scaled up without excessive numbering-up is necessary. A further scale-up of the RDBER is conceivable as well: While the diameter of the electrode discs is limited mainly by the angular velocity at the outer edge, the shaft can be extended (and equipped with more electrodes) until it is unable to statically support its own weight.

Funding

This work was supported by a grant of the Federal Ministry of Education and Research (BMBF) as part of the BioElectroPlast project, no. 033RC006.

Declaration of Competing Interest

The authors declare that they have no known competing financial interests or personal relationships that could have appeared to influence the work reported in this paper.

Acknowledgements

Special thanks go to Prof. Harald Horn for the initial idea behind the reactor concept, to Axel Heidt as the person responsible for the IC measurements and to Erwin Wachter, Joachim Lang and Alfred Herbst from the metal workshop of the EBI for their work and support during the construction of the reactor.

CRediT authorship contribution statement

Max Hackbarth: Investigation, Conceptualization, Methodology, Visualization. **Johannes Gescher:** Conceptualization, Writing - Review & Editing, Funding acquisition. **Harald Horn:** Conceptualization, Writing - Review & Editing, Funding acquisition. **Johannes Eberhard**

654 **Reiner:** Investigation, Conceptualization, Methodology, Visualization, Writing - Original Draft
655 & Editing.

656

657 ## References

658 Barham, P.J., Keller, A., Otun, E.L., Holmes, P.A., 1984. Crystallization and morphology of a bacterial
659 thermoplastic: poly-3-hydroxybutyrate. J Mater Sci 19, 2781–2794.
660 https://doi.org/10.1007/BF01026954

661 Bauer, A., Wagner, M., Saravia, F., Bartl, S., Hilgenfeldt, V., Horn, H., 2019. In-situ monitoring and
662 quantification of fouling development in membrane distillation by means of optical coherence
663 tomography. J Memb Sci 577, 145–152. https://doi.org/10.1016/j.memsci.2019.02.006

664 Cabau-Peinado, O., Straathof, A.J.J., Jourdin, L., 2021. A General Model for Biofilm-Driven Microbial
665 Electrosynthesis of Carboxylates From CO_2. Front Microbiol 12, 1405.
666 https://doi.org/10.3389/FMICB.2021.669218/BIBTEX

667 Cheng, K.Y., Ho, G., Cord-Ruwisch, R., 2012. Energy-efficient treatment of organic wastewater streams
668 using a rotatable bioelectrochemical contactor (RBEC). Bioresour Technol 126, 431–436.
669 https://doi.org/10.1016/J.BIORTECH.2011.12.011

670 Cheng, K.Y., Ho, G., Cord-Ruwisch, R., 2011. Novel methanogenic rotatable bioelectrochemical system
671 operated with polarity inversion. Environ Sci Technol 45, 796–802.
672 https://doi.org/10.1021/ES102482J/SUPPL_FILE/ES102482J_SI_001.PDF

673 Christodoulou, X., Velasquez-Orta, S.B., 2016. Microbial Electrosynthesis and Anaerobic Fermentation:
674 An Economic Evaluation for Acetic Acid Production from CO_2 and CO. Environ Sci Technol 50,
675 11234–11242. https://doi.org/10.1021/acs.est.6b02101

676 Cortez, S., Teixeira, P., Oliveira, R., Mota, M., 2008. Rotating biological contactors: A review on main
677 factors affecting performance. Rev Environ Sci Biotechnol 7, 155–172.
678 https://doi.org/10.1007/S11157-008-9127-X/TABLES/4

679 Cotterill, S.E., Dolfing, J., Jones, C., Curtis, T.P., Heidrich, E.S., 2017. Low Temperature Domestic
680 Wastewater Treatment in a Microbial Electrolysis Cell with 1 m^2 Anodes: Towards System Scale-
681 Up. Fuel Cells 17, 584–592. https://doi.org/10.1002/fuce.201700034

682 Cusick, R.D., Bryan, B., Parker, D.S., Merrill, M.D., Mehanna, M., Kiely, P.D., Liu, G., Logan, B.E., 2011.
683 Performance of a pilot-scale continuous flow microbial electrolysis cell fed winery wastewater.
684 Appl Microbiol Biotechnol 89, 2053–2063. https://doi.org/10.1007/S00253-011-3130-9

685 de Beer, D., Stoodley, P., Roe, F., Lewandowski, Z., 1994. Effects of biofilm structures on oxygen
686 distribution and mass transport. Biotechnol Bioeng 43, 1131–1138.
687 https://doi.org/10.1002/BIT.260431118

688 Edel, M., Philipp, L.-A., Lapp, J., Reiner, J., Gescher, J., 2022. Electron transfer of extremophiles in
689 bioelectrochemical systems. Extremophiles 26, 31. https://doi.org/10.1007/s00792-022-01279-
690 8

691 Engel, C., Schattenberg, F., Dohnt, K., Schröder, U., Müller, S., Krull, R., 2019. Long-Term Behavior of
692 Defined Mixed Cultures of *Geobacter sulfurreducens* and *Shewanella oneidensis* in
693 Bioelectrochemical Systems. Front Bioeng Biotechnol 7, 60.
694 https://doi.org/10.3389/fbioe.2019.00060

695 Enzmann, F., Mayer, F., Stöckl, M., Mangold, K.M., Hommel, R., Holtmann, D., 2019a. Transferring
696 bioelectrochemical processes from H-cells to a scalable bubble column reactor. Chem Eng Sci 193,
697 133–143. https://doi.org/10.1016/J.CES.2018.08.056

698 Enzmann, F., Stöckl, M., Zeng, A.-P., Holtmann, D., 2019b. Same but different-Scale up and numbering
699 up in electrobiotechnology and photobiotechnology. Eng Life Sci 19, 121–132.
700 https://doi.org/10.1002/elsc.201800160

701 Gil-Carrera, L., Escapa, A., Mehta, P., Santoyo, G., Guiot, S.R., Morán, A., Tartakovsky, B., 2013.
702 Microbial electrolysis cell scale-up for combined wastewater treatment and hydrogen
703 production. Bioresour Technol 130, 584–591. https://doi.org/10.1016/j.biortech.2012.12.062

704 Gildemyn, S., Verbeeck, K., Jansen, R., Rabaey, K., 2017. The type of ion selective membrane
705 determines stability and production levels of microbial electrosynthesis. Bioresour Technol 224,
706 358–364. https://doi.org/10.1016/J.BIORTECH.2016.11.088

707 Guo, K., Prévoteau, A., Patil, S.A., Rabaey, K., 2015. Engineering electrodes for microbial
708 electrocatalysis. Curr Opin Biotechnol 33, 149–156.
709 https://doi.org/10.1016/J.COPBIO.2015.02.014

710 Guo, K., Prévoteau, A., Rabaey, K., 2017. A novel tubular microbial electrolysis cell for high rate
711 hydrogen production. J Power Sources 356, 484–490.
712 https://doi.org/10.1016/J.JPOWSOUR.2017.03.029

713 Hackbarth, M., Jung, T., Reiner, J.E., Gescher, J., Horn, H., Hille-Reichel, A., Wagner, M., 2020.
714 Monitoring and quantification of bioelectrochemical *Kyrpidia spormannii* biofilm development in
715 a novel flow cell setup. Chem Eng J 390, 124604. https://doi.org/10.1016/j.cej.2020.124604

716 Hassard, F., Biddle, J., Cartmell, E., Jefferson, B., Tyrrel, S., Stephenson, T., 2015. Rotating biological
717 contactors for wastewater treatment – A review. Process Saf Environ 94, 285–306.
718 https://doi.org/10.1016/J.PSEP.2014.07.003

719 Horn, H., Morgenroth, E., 2006. Transport of oxygen, sodium chloride, and sodium nitrate in biofilms.
720 Chem Eng Sci 61, 1347–1356. https://doi.org/10.1016/J.CES.2005.08.027

721 Huang, L., Tian, F., Pan, Y., Shan, L., Shi, Y., Logan, B.E., 2019. Mutual benefits of acetate and mixed
722 tungsten and molybdenum for their efficient removal in 40 L microbial electrolysis cells. Water
723 Res 162, 358–368. https://doi.org/10.1016/j.watres.2019.07.003

724 Jourdin, L., Burdyny, T., 2021. Microbial Electrosynthesis: Where Do We Go from Here? Trends
725 Biotechnol 39, 359–369. https://doi.org/10.1016/J.TIBTECH.2020.10.014

726 Jourdin, L., Sousa, J., Stralen, N. van, Strik, D.P.B.T.B., 2020. Techno-economic assessment of microbial
727 electrosynthesis from CO_2 and/or organics: An interdisciplinary roadmap towards future research
728 and application. Appl Energ 279, 115775. https://doi.org/10.1016/J.APENERGY.2020.115775

729 Jung, T., Hackbarth, M., Horn, H., Gescher, J., 2020. Improving the Cathodic Biofilm Growth Capabilities
730 of *Kyrpidia spormannii* EA-1 by Undirected Mutagenesis. Microorganisms 9, 77.
731 https://doi.org/10.3390/microorganisms9010077

732 Kerzenmacher, S., 2017. Engineering of Microbial Electrodes. Springer, Berlin, Heidelberg, pp. 135–
733 180. https://doi.org/10.1007/10_2017_16

734 Korth, B., Harnisch, F., 2019. Spotlight on the energy harvest of electroactive microorganisms: The
735 impact of the applied anode potential. Front Microbiol 10, 1352.
736 https://doi.org/10.3389/FMICB.2019.01352/BIBTEX

737 Kracke, F., Lai, B., Yu, S., Krömer, J.O., 2018. Balancing cellular redox metabolism in microbial
738 electrosynthesis and electro fermentation – A chance for metabolic engineering. Metab Eng 45,
739 109–120. https://doi.org/10.1016/j.ymben.2017.12.003

740 Krieg, T., Phan, L.M.P., Wood, J.A., Sydow, A., Vassilev, I., Krömer, J.O., Mangold, K.M., Holtmann, D.,
741 2018a. Characterization of a membrane-separated and a membrane-less electrobioreactor for
742 bioelectrochemical syntheses. Biotechnol Bioeng 115, 1705–1716.
743 https://doi.org/10.1002/BIT.26600

744 Krieg, Thomas, Madjarov, Joana, Rosa, Luis F M, Enzmann, Franziska, Harnisch, Falk, Holtmann, Dirk,
745 Rabaey, Korneel, Krieg, T, Enzmann, F, Holtmann, D, Madjarov, J, Rosa, L F M, Harnisch, F, Rabaey,
746 K, 2018b. Reactors for Microbial Electrobiotechnology. Adv Biochem Eng Biotechnol 167, 231–
747 271. https://doi.org/10.1007/10_2017_40

748 Lieder, M., Rashid, A., 2016. Towards circular economy implementation: A comprehensive review in
749 context of manufacturing industry. J Clean Prod 115, 36–51.
750 https://doi.org/10.1016/j.jclepro.2015.12.042

751 Logan, B.E., Rossi, R., Ragab, A., Saikaly, P.E., 2019. Electroactive microorganisms in bioelectrochemical
752 systems. Nat Rev Microbiol 17, 307–319. https://doi.org/10.1038/s41579-019-0173-x

753 Nevin, K.P., Woodard, T.L., Franks, A.E., Summers, Z.M., Lovley, D.R., 2010. Microbial electrosynthesis:
754 Feeding microbes electricity to convert carbon dioxide and water to multicarbon extracellular
755 organic compounds. mBio 1, e00103-10. https://doi.org/10.1128/mBio.00103-10

756 Park, S.-G., Rajesh, P.P., Sim, Y.-U., Jadhav, D.A., Noori, Md.T., Kim, D.-H., Al-Qaradawi, S.Y., Yang, E.,
757 Jang, J.-K., Chae, K.-J., 2022. Addressing scale-up challenges and enhancement in performance of
758 hydrogen-producing microbial electrolysis cell through electrode modifications. Energy Reports
759 8, 2726–2746. https://doi.org/10.1016/j.egyr.2022.01.198

760 Pillot, G., Sunny, S., Comes, V., Heussner, A., Kerzenmacher, S., 2022a. Effect of cathode properties on
761 the thermophilic electrosynthesis of PolyHydroxyAlkanoates by *Kyrpidia spormannii*. Bioresour
762 Technol Rep 18, 101040. https://doi.org/10.1016/J.BITEB.2022.101040

763 Pillot, G., Sunny, S., Comes, V., Kerzenmacher, S., 2022b. Optimization of growth and electrosynthesis
764 of PolyHydroxyAlkanoates by the thermophilic bacterium *Kyrpidia spormannii*. Bioresour Technol
765 Rep 17, 100949. https://doi.org/10.1016/J.BITEB.2022.100949

766 Prévoteau, A., Carvajal-Arroyo, J.M., Ganigué, R., Rabaey, K., 2020. Microbial electrosynthesis from
767 CO_2: forever a promise? Curr Opin Biotechnol 62, 48–57.
768 https://doi.org/10.1016/j.copbio.2019.08.014

769 Rader, G.K., Logan, B.E., 2010. Multi-electrode continuous flow microbial electrolysis cell for biogas
770 production from acetate. Int J Hydrogen Energy 35, 8848–8854.
771 https://doi.org/10.1016/j.ijhydene.2010.06.033

772 Reiner, J.E., Geiger, K., Hackbarth, M., Fink, M., Lapp, C.J., Jung, T., Dötsch, A., Hügler, M., Wagner, M.,
773 Hille-Reichel, A., Wilcke, W., Kerzenmacher, S., Horn, H., Gescher, J., 2020. From an extremophilic

community to an electroautotrophic production strain: identifying a novel Knallgas bacterium as cathodic biofilm biocatalyst. ISME J 14, 1125–1140. https://doi.org/10.1038/s41396-020-0595-5

Reiner, J.E., Jung, T., Lapp, C.J., Siedler, M., Bunk, B., Overmann, J., Gescher, J., 2018a. *Kyrpidia spormannii* sp. nov., a thermophilic, hydrogenoxidizing, facultative autotroph, isolated from hydrothermal systems at São Miguel Island, and emended description of the genus *Kyrpidia*. Int J Syst Evol Microbiol 68, 3735–3740. https://doi.org/10.1099/IJSEM.0.003037/CITE/REFWORKS

Reiner, J.E., Lapp, C.J., Bunk, B., Spröer, C., Overmann, J., Gescher, J., 2018b. Complete Genome Sequence of *Kyrpidia* sp. Strain EA-1, a Thermophilic Knallgas Bacterium, Isolated from the Azores. Genome Announc 6, e01505-17. https://doi.org/10.1128/genomeA.01505-17

Rodziewicz, J., Mielcarek, A., Janczukowicz, W., Jóźwiak, T., Struk – Sokołowska, J., Bryszewski, K., 2019. The share of electrochemical reduction, hydrogenotrophic and heterotrophic denitrification in nitrogen removal in rotating electrobiological contactor (REBC) treating wastewater from soilless cultivation systems. Science of The Total Environment 683, 21–28. https://doi.org/10.1016/J.SCITOTENV.2019.05.239

Sayess, R.R., Saikaly, P.E., El-Fadel, M., Li, D., Semerjian, L., 2013. Reactor performance in terms of COD and nitrogen removal and bacterial community structure of a three-stage rotating bioelectrochemical contactor. Water Res 47, 881–894. https://doi.org/10.1016/J.WATRES.2012.11.023

Schneider, C.A., Rasband, W.S., Eliceiri, K.W., 2012. NIH Image to ImageJ: 25 years of image analysis. Nat Methods 9, 671–675. https://doi.org/10.1038/nmeth.2089

Singh, L., Miller, A.G., Wang, L., Liu, H., 2021. Scaling-up up-flow microbial electrolysis cells with a compact electrode configuration for continuous hydrogen production. Bioresour Technol 331, 125030. https://doi.org/10.1016/j.biortech.2021.125030

Utesch, T., Zeng, A.P., 2018. A novel All-in-One electrolysis electrode and bioreactor enable better study of electrochemical effects and electricity-aided bioprocesses. Eng Life Sci 18, 600. https://doi.org/10.1002/ELSC.201700198

van den Berg, L., Kirkland, C.M., Seymour, J.D., Codd, S.L., van Loosdrecht, M.C.M., de Kreuk, M.K., 2020. Heterogeneous diffusion in aerobic granular sludge. Biotechnol Bioeng 117, 3809. https://doi.org/10.1002/BIT.27522

Vassilev, I., Dessì, P., Puig, S., Kokko, M., 2022. Cathodic biofilms – A prerequisite for microbial electrosynthesis. Bioresour Technol 348, 126788. https://doi.org/10.1016/j.biortech.2022.126788

Wagner, M., Horn, H., 2017. Optical coherence tomography in biofilm research: A comprehensive review. Biotechnol Bioeng 114, 1386–1402. https://doi.org/10.1002/BIT.26283

Wang, L., Long, F., Liang, D., Xiao, X., Liu, H., 2021. Hydrogen production from lignocellulosic hydrolysate in an up-scaled microbial electrolysis cell with stacked bio-electrodes. Bioresour Technol 320, 124314. https://doi.org/10.1016/j.biortech.2020.124314

Wood, J.C., Grové, J., Marcellin, E., Heffernan, J.K., Hu, S., Yuan, Z., Virdis, B., 2021. Strategies to improve viability of a circular carbon bioeconomy-A techno-economic review of microbial electrosynthesis and gas fermentation. Water Res 201, 117306. https://doi.org/10.1016/j.watres.2021.117306

Zeppilli, M., Lai, A., Villano, M., Majone, M., 2016. Anion vs cation exchange membrane strongly affect mechanisms and yield of CO_2 fixation in a microbial electrolysis cell. Chem Eng J 304, 10–19. https://doi.org/10.1016/J.CEJ.2016.06.020

Zhang, S., Jiang, J., Wang, H., Li, F., Hua, T., Wang, W., 2021. A review of microbial electrosynthesis applied to carbon dioxide capture and conversion: The basic principles, electrode materials, and bioproducts. J CO2 Util 51, 101640. https://doi.org/10.1016/j.jcou.2021.101640